

## Particle morphology effects in random sequential adsorption

Lj. Budinski-Petković,<sup>1</sup> I. Lončarević,<sup>1</sup> D. Dujak,<sup>2</sup> A. Karač,<sup>3</sup> J. R. Šćepanović,<sup>4</sup> Z. M. Jakšić,<sup>4</sup> and S. B. Vrhovac<sup>4,\*</sup>

<sup>1</sup>Faculty of Engineering, Trg D. Obradovića 6, Novi Sad 21000, Serbia

<sup>2</sup>Faculty of Metallurgy and Materials, University of Zenica, Zenica, Bosnia and Herzegovina

<sup>3</sup>Polytechnic Faculty, University of Zenica, Zenica, Bosnia and Herzegovina

<sup>4</sup>Scientific Computing Laboratory, Center for the Study of Complex Systems, Institute of Physics Belgrade, University of Belgrade, Pregrevica 118, Zemun 11080, Belgrade, Serbia

(Received 12 October 2016; published 13 February 2017)

The properties of the random sequential adsorption of objects of various shapes on a two-dimensional triangular lattice are studied numerically by means of Monte Carlo simulations. The depositing objects are formed by self-avoiding lattice steps, whereby the size of the objects is gradually increased by wrapping the walks in several different ways. The aim of this work is to investigate the impact of the geometrical properties of the shapes on the jamming density  $\theta_j$  and on the temporal evolution of the coverage fraction  $\theta(t)$ . Our results suggest that the order of symmetry axis of a shape exerts a decisive influence on adsorption kinetics near the jamming limit  $\theta_j$ . The decay of probability for the insertion of a new particle onto a lattice is described in a broad range of the coverage  $\theta$  by the product between the linear and the stretched exponential function for all examined objects. The corresponding fitting parameters are discussed within the context of the shape descriptors, such as rotational symmetry and the shape factor (parameter of nonsphericity) of the objects. Predictions following from our calculations suggest that the proposed fitting function for the insertion probability is consistent with the exponential approach of the coverage fraction  $\theta(t)$  to the jamming limit  $\theta_j$ .

DOI: [10.1103/PhysRevE.95.022114](https://doi.org/10.1103/PhysRevE.95.022114)

### I. INTRODUCTION

Understanding various aspects of random sequential adsorption (RSA) has a great scientific and industrial importance as it has been linked to a wide range of applications in biology, nanotechnology, device physics, physical chemistry, and materials science [1–4]. Depositing objects range in size from micrometer scale down to nanometer scale, and depending on the application in question, the objects could be colloidal particles, polymer chains, globular proteins, nanotubes, DNA segments, or general geometrical shapes, such as disks, polygons, etc.

The RSA model adsorption process considers sequential addition of particles on the  $n$ -dimensional substrate such that at each time step only one particle is added on the substrate at a randomly selected position. During the process of addition, newly added particles are forbidden from overlapping with the already adsorbed particles, and any attempt of adsorption resulting in an overlap is rejected. The adsorbed particles are permanently fixed at their spatial positions so that they affect the geometry of all later placements. This leads to slowing of the rate of adsorption due to unavailability of the surface for further addition. The most common parameter to characterize the kinetic properties of a deposition process is the coverage  $\theta(t)$ , defined as the ratio of the number of occupied sites at time  $t$  and the total number of sites. Due to the blocking of the substrate area by the already randomly adsorbed particles, at large times the coverage  $\theta(t)$  approaches the jammed-state value  $\theta_j$ , where only gaps too small to fit new particles are left in the monolayer.

The RSA models are broadly classified into continuum models and lattice models on the basis of the nature of the

substrate. The long-term behavior of the coverage fraction  $\theta(t)$  is known to be asymptotically algebraic for continuum systems [5–8] and exponential for lattice models [9–12]. For the latter case the approach of the coverage fraction  $\theta(t)$  to its jamming limit  $\theta_j$  is given by the time dependence:

$$\theta_j - \theta(t) \sim \exp(-t/\sigma), \quad (1)$$

where parameters  $\theta_j$  and  $\sigma$  depend on the shape, orientational freedom of depositing objects, and the dimensionality of the substrate [11,12].

An important issue in RSA is the influence of the shape of depositing objects on kinetics of irreversible deposition and on the morphological characteristics of coverings. RSA of many different geometric objects has been studied for both continuum and lattice models in order to determine the significance of particle anisotropy in formation of the jammed-state coverings. For this purpose, the jamming coverings generated by RSA on continuous substrates have been analyzed for depositing particles of various shapes, such as spherocylinders and ellipsoids [13,14], rectangles [15,16], starlike particles [17,18], and polymers [19,20]. Results obtained for anisotropic particles show that jamming coverage reaches its maximum when the long-to-short particle axis ratio is approximately 1.5–2.0 [13,16]. Recently Cieřla *et al.* have performed an extensive numerical simulation of the RSA of smoothed  $n$ -mers, spherocylinders, and ellipses [21–23] in order to find a shape which maximizes the jamming coverage. It is found that the highest packing fraction is obtained for ellipses having the long-to-short axis ratio of 1.85, which is the largest anisotropy among the investigated shapes.

The kinetics of the deposition process is strongly dependent on geometrical properties of the objects. For instance, Khandkar *et al.* [24] have studied RSA of zero-area symmetric angled objects on a continuum substrate for the full range

\*vrhovac@ipb.ac.rs; <http://www.ipb.ac.rs/~vrhovac/>

( $0^\circ$ – $180^\circ$ ) of values of the arm angle  $\phi$  and have observed that  $\theta_j - \theta(t) \sim t^\alpha$  as expected. Value of the exponent  $\alpha$  exhibits a crossover near  $\phi = 0^\circ$  or  $180^\circ$  and is significantly lower in the case of the angled objects than in the case of needles.

Formation of random deposits of extended objects on discrete substrates and their properties have been extensively studied in many different contexts and using a number of different tools, including irreversible deposition [11,25,26], an adsorption-desorption model [27–29], random deposition with diffusional relaxation [30–32], and percolations [33–35].

Wang and Pandey [36] have studied the kinetics and jamming coverage in RSA of self-avoiding walk chains on a square lattice and found that the jamming coverage  $\theta_j$  decreases with the chain length with a power law. They observed a crossover from a power-law variation of the coverage fraction  $\theta(t)$  in the intermediate time regime to an exponential growth in the long time, especially for short chains.

Budinski and Kozmidis [11,26] have carried out extensive simulations of irreversible deposition using objects of different sizes and rotational symmetries on a square and triangular lattice. They reported that shapes with the symmetry axis of a higher order have lower values of  $\sigma$  [Eq. (1)], i.e., they approach their jamming limit more rapidly. This confirms the crucial role of the geometrical character of the objects in deposition dynamics.

The main goal of the present study is to extend the analysis in Ref. [11] to large collections of objects of various shapes that can be made by self-avoiding random walks on a triangular lattice. The large number of examined objects represents a good basis for testing the impact of the geometrical properties of the shapes on the jamming density  $\theta_j$  and on the temporal evolution of the coverage fraction  $\theta(t)$ . We address the following questions regarding the influence of the shape on the rapidity of the approach to the jamming state. First, we investigate the interplay between the size and the symmetry properties of depositing shapes. This is an important question because the slowing of the dynamics in the RSA model can be understood as a consequence of steric effects that make certain insertions of particles infeasible owing to an effective high local density on the lattice. Second, we analyze whether there is some intrinsic property of the objects that, in addition to symmetry, also promotes or suppresses rare adsorption events which take place on isolated islands of connected unoccupied sites at the late times of the deposition process.

For this purpose we use the concept of the shape factor to measure the circularity of depositing objects. The shape factor (parameter of nonsphericity) was introduced by Moučka and Nezbeda [37], for tracking the change in structure as a liquid-like system approaches a disordered jammed state. Shape factor,  $\zeta$ , is defined as the degree to which a particle is similar to a circle, taking into consideration the smoothness of the perimeter. This means the parameter  $\zeta$  is a measurement of both the particle form and roughness. Thus, the farther away from a perfectly round and smooth circle that a particle becomes, the higher the  $\zeta$  value. The shape factor is a dimensionless value. Moreover, we generalize the definition of the shape factor for planar geometric figures [see Eq. (6)] to make it applicable to the objects made by directed self-avoiding walks on the two-dimensional lattice.

In this paper the shape factor  $\zeta$  is associated with the evolution of probability for the insertion of a new particle onto a lattice during the deposition process. This work provides a closer insight into the behavior of the insertion probability during the irreversible deposition of extended objects. The decay of the insertion probability is described in a broad range of the coverage  $\theta$  by the product between linear and stretched exponential function for all examined objects. We discuss the fitting parameters from the proposed fitting function within the context of the shape descriptors, such as rotational symmetry and shape factor of the objects.

The paper is organized as follows. Section II describes the details of the simulations. The approach of the coverage fraction  $\theta(t)$  to the jamming limit  $\theta_j$  is analyzed in Sec. III A. Section III B is devoted to the analysis of the behavior of probability for the insertion of a particle onto a lattice during the deposition process. Finally, Sec. IV contains some additional comments and final remarks.

## II. DEFINITION OF THE MODEL AND THE SIMULATION METHOD

The depositing objects are modeled by self-avoiding walks on the planar triangular lattice. A self-avoiding shape of length  $\ell$  is a sequence of *distinct* vertices  $(\omega_0, \dots, \omega_\ell)$  such that each vertex is a nearest neighbor of its predecessor, i.e., a walk of length  $\ell$  covers  $j = \ell + 1$  lattice sites. Starting from a dimer, size of the objects is gradually increased by wrapping the walks in several different ways. Formation of wrapping triangles  $T_j$  is shown in Table I. In a similar way, rhombuses  $R_j$  and hexagons  $H_j$  of larger sizes  $j = 2, 3, \dots, 30$  are obtained by wrapping as shown in Tables II and III, respectively. In this manner, wrapping objects of larger sizes occupy all comprised sites on the lattice.

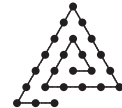
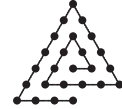
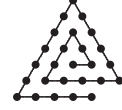
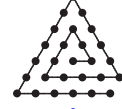
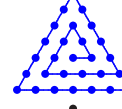
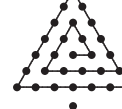
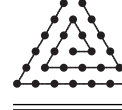
On a triangular lattice objects with a symmetry axis of first, second, third, and sixth order can be formed. Rotational symmetry of order  $n_s$ , also called  $n$ -fold rotational symmetry, with respect to a particular axis perpendicular to the triangular lattice, means that rotation by an angle of  $2\pi/n_s$  does not change the object. The values of the order of symmetry axis  $n_s$  are given in Tables I–III for all wrapping triangles, rhombuses, and hexagons. We concentrate here on the influence of the order of symmetry axis of the shape on the kinetics of the adsorption process. Special attention is paid to the comparison of the results for lattice objects of different rotational symmetries but of the same number of segments.

At each Monte Carlo step a lattice site is selected at random. If the selected site is unoccupied, we fix the beginning of the walk that makes the chosen shape  $T_j$  (or  $R_j, H_j$ ) at this site. Then we randomly pick one of the six possible orientations on the lattice with equal probability, start the corresponding  $\ell$ -step walk in that direction, and search whether all successive  $\ell$  sites are unoccupied. If so, we occupy these  $j = \ell + 1$  sites and place the object. If the attempt fails, a new site and a new direction are selected at random. This scheme is usually called the conventional or standard model of RSA. The other strategy to perform an RSA, where we check all possible directions from the selected site, is named the end-on model [11]. The jamming limit is reached when no more objects can be placed in any position on the lattice. Since the local domain

TABLE I. Wrapping triangles,  $T_j$ . The colors are associated with different order  $n_s$  of the symmetry axis. For each shape,  $\theta_j$  is the jamming coverage and  $\sigma$  is the relaxation time [Eq. (1)].

Shape ( $T_j$ )	$j$	$n_s$	$\sigma$	$\theta_j$
	2	2	3.03	0.9141
	3	3	1.97	0.7969
	4	1	5.99	0.7741
	5	1	6.01	0.7605
	6	3	2.04	0.7210
	7	1	5.97	0.6901
	8	1	6.09	0.6993
	9	1	5.99	0.7101
	10	3	2.00	0.6816
	11	1	5.83	0.6493
	12	1	5.71	0.6624
	13	1	5.97	0.6683
	14	1	5.94	0.6816
	15	3	2.01	0.6572
	16	1	5.81	0.6263
	17	1	5.80	0.6368
	18	1	6.05	0.6445
	19	1	5.95	0.6518
	20	1	5.90	0.6633
	21	3	1.99	0.6407
	22	1	5.56	0.6119
	23	1	6.05	0.6197

TABLE I. (Continued.)

Shape ( $T_j$ )	$j$	$n_s$	$\sigma$	$\theta_j$
	24	1	5.89	0.6286
	25	1	5.98	0.6323
	26	1	5.79	0.6406
	27	1	5.92	0.6498
	28	3	1.93	0.6286
	29	1	5.86	0.6016
	30	1	5.92	0.6079

structures for the end-on model are more dense than those of the conventional model, the jamming limit  $\theta_j$  for the end-on model is slightly larger than that for the conventional model.

It is well established that correlations in RSA decay extremely fast [1,6,38]. Therefore, one can obtain high-precision results numerically on relatively small lattices, without worrying about finite-size effects [39–41] and averaging over not too many runs because the system is self-averaging. Numerical studies have shown that the finite-size effects on the lattice of size  $L$  can be neglected for object sizes  $\leq L/8$  [10]. Consequently, Monte Carlo simulations are performed on a triangular lattice of size  $L = 240$ . Periodic boundary conditions are used in all directions. The time  $t$  is counted by the number of attempts to select a lattice site and scaled by the total number of lattice sites  $N = L^2 = 57\,600$ . The simulation data are averaged over 1000 independent runs for each depositing object.

### III. RESULTS AND DISCUSSION

#### A. Particle jamming and late-stage deposition kinetics

First, we report and discuss the numerical results regarding the influence of the order of the symmetry axis of the shape on the kinetics of the deposition processes. The simulations have been performed for all wrapping triangles, rhombuses, and hexagons from Tables I–III. Figure 1 shows the plots of  $\ln[\theta_j - \theta(t)]$  versus  $t$  for three wrapping triangles ( $T_3$ ,  $T_4$ ,  $T_6$ ) and hexagons ( $H_4$ ,  $H_7$ ,  $H_{19}$ ), and for two wrapping rhombuses

TABLE II. Wrapping rhombuses,  $R_j$ . The colors are associated with different order  $n_s$  of the symmetry axis. For each shape,  $\theta_j$  is the jamming coverage and  $\sigma$  is the relaxation time [Eq. (1)].

Shape ( $R_j$ )	$j$	$n_s$	$\sigma$	$\theta_j$
	2	2	3.02	0.9141
	3	1	6.03	0.8345
	4	2	3.08	0.7591
	5	1	6.00	0.7605
	6	2	3.00	0.7299
	7	1	5.98	0.7075
	8	1	6.01	0.6956
	9	2	2.99	0.6792
	10	1	5.98	0.6706
	11	1	5.78	0.6885
	12	2	2.90	0.6716
	13	1	6.01	0.6506
	14	1	6.04	0.6531
	15	1	6.01	0.6463
	16	2	2.99	0.6428
	17	1	6.02	0.6332
	18	1	6.00	0.6439
	19	1	5.72	0.6549
	20	2	2.97	0.6416
	21	1	5.79	0.6224
	22	1	5.99	0.6258
	23	1	5.78	0.6254
	24	1	6.02	0.6226
	25	2	2.79	0.6220
	26	1	5.95	0.6126
	27	1	5.90	0.6199

TABLE II. (*Continued.*)

Shape ( $R_j$ )	$j$	$n_s$	$\sigma$	$\theta_j$
	28	1	5.71	0.6260
	29	1	5.97	0.6349
	30	2	3.10	0.6236

( $R_3$ ,  $R_6$ ), so that it contains results for shapes of all symmetry orders. Lines with four different slopes are plotted in Fig. 1, showing the late times of the deposition process corresponding to objects of different symmetry order,  $n_s = 1, 2, 3, 6$ , as indicated in the legend. Following the objects formed by walks of increasing length (e.g.,  $T_3$  and  $T_4$ ), we can see that objects differing in only one self-avoiding lattice step can have significantly different values of the relaxation time  $\sigma$ . On the other hand, for a given value of symmetry order  $n_s$ , these plots are parallel lines in the late stages of the deposition process for shapes of very different lengths (e.g.,  $H_7$  and  $H_{19}$ ). This means that for a given  $n_s$ , rapidity of the approach to the jamming state is not affected by the length of the shape. Consequently, order of symmetry of the shape has an essential influence in the late times of the deposition process. To further confirm this notion, we have calculated the values of the parameter  $\sigma$  [Eq. (1)] from the slopes of the  $\ln[\theta_j - \theta(t)]$  versus  $t$  curves in the late times of the process. Parameter  $\sigma$  determines how fast the lattice is filled up to the jamming coverage  $\theta_j$ . The values of relaxation time  $\sigma$  are given in Tables I–III for all examined

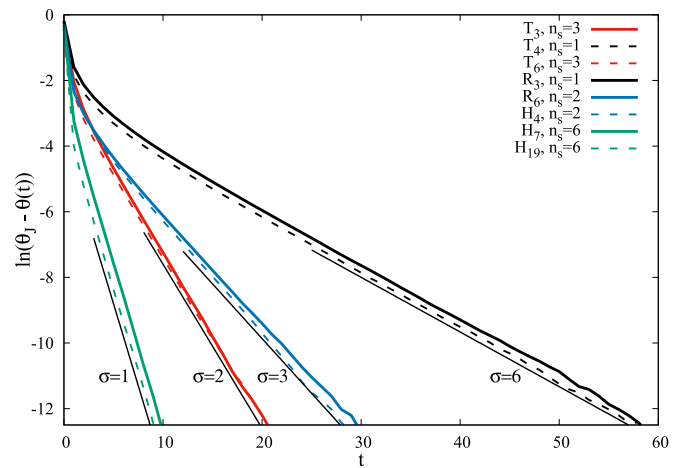


FIG. 1. Plots of  $\ln(\theta_j - \theta(t))$  vs  $t$  for wrapping triangles  $T_3$ ,  $T_4$ ,  $T_6$ , rhombuses  $R_3$ ,  $R_6$ , and hexagons  $H_4$ ,  $H_7$ ,  $H_{19}$  from Tables I–III. The curves correspond to various values of the order of symmetry axis of the shape,  $n_s$ , as indicated in the legend. Additionally, the slanted straight lines with the slope  $-1/\sigma = -1, -1/2, -1/3, -1/6$  are shown, indicating the late-time RSA behavior and are guides for the eye.

TABLE III. Wrapping hexagons,  $H_j$ . The colors are associated with different order  $n_s$  of the symmetry axis. For each shape,  $\theta_j$  is the jamming coverage and  $\sigma$  is the relaxation time [Eq. (1)].

Shape ( $H_j$ )	$j$	$n_s$	$\sigma$	$\theta_j$
	2	2	2.99	0.9141
	3	3	1.99	0.7970
	4	2	2.94	0.7591
	5	1	6.01	0.7604
	6	1	6.00	0.7347
	7	6	0.98	0.6697
	8	1	5.78	0.6923
	9	1	5.99	0.6857
	10	2	2.97	0.6813
	11	1	6.00	0.6665
	12	3	2.01	0.6508
	13	1	5.98	0.6431
	14	2	3.00	0.6457
	15	1	5.99	0.6433
	16	1	6.00	0.6623
	17	1	6.05	0.6472
	18	1	6.01	0.6367
	19	6	1.02	0.6147
	20	1	6.05	0.6163
	21	1	5.79	0.6352
	22	1	6.01	0.6265
	23	1	6.03	0.6293
	24	2	2.98	0.6327

TABLE III. (Continued.)

Shape ( $H_j$ )	$j$	$n_s$	$\sigma$	$\theta_j$
	25	1	6.01	0.6204
	26	1	5.94	0.6190
	27	3	2.01	0.6136
	28	1	5.98	0.6057
	29	1	5.76	0.6099
	30	2	2.83	0.6119

objects. Approximate values of the parameter  $\sigma$  for the four classes of objects of different symmetry are found to be the following:

- $\sigma \simeq 6.0$  for the shapes with a symmetry axis of first order,  $n_s = 1$ ;
- $\sigma \simeq 3.0$  for the shapes with a symmetry axis of second order,  $n_s = 2$ ;
- $\sigma \simeq 2.0$  for the shapes with a symmetry axis of third order,  $n_s = 3$ ;
- $\sigma \simeq 1.0$  for the shapes with a symmetry axis of sixth order,  $n_s = 6$ .

This means that the approach to the jamming limit is faster for more regular and symmetric shapes. At large times, adsorption events take place on islands of unoccupied sites. The individual islands act as selective targets for specific deposition events. In other words, there is only a restricted number of possible orientations in which an object can reach a vacant location, provided the location is small enough. For a shape of a higher order of symmetry  $n_s$ , there is a greater number of possible orientations for deposition into a selective target on the lattice. Hence, the increase of the order of symmetry of the shape enhances the rate of single particle adsorption. This shortens the mean waiting time between consecutive deposition events and the approach to the jamming state is faster.

Figures 2(a)–2(c) show the dependence of the jamming coverage  $\theta_j$  on the number  $j$  of sites covered by an object for wrapping triangles (a), rhombuses (b), and hexagons (c). Numerical values of the obtained jamming coverages  $\theta_j$  are also given in Tables I–III for all examined wrapping shapes.

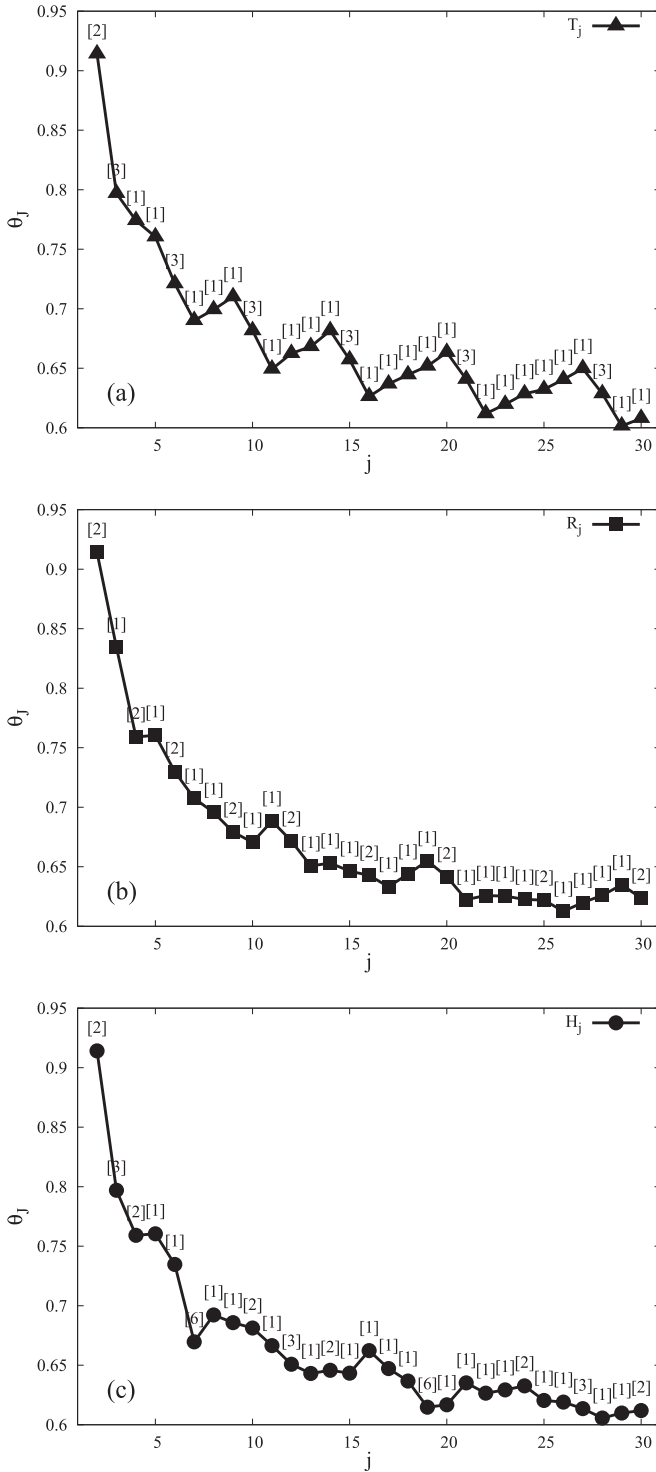


FIG. 2. Jamming coverages  $\theta_j$  for all wrapping (a) triangles  $T_j$ , (b) rhombuses  $R_j$ , and (c) hexagons  $H_j$ , from Tables I–III. Here  $j = 2, \dots, 30$  denotes the number of sites covered by an object. Numerical values of the symmetry order  $n_s$  of the shapes are given in the square brackets above the corresponding plot symbols.

From Fig. 2 it is evident that for small values of  $j \lesssim 7$ , jamming coverages  $\theta_j$  decrease very rapidly with the size of the objects. A noticeable drop in the jamming coverage  $\theta_j$  is thus a clear consequence of the enhanced frustration of the spatial

adsorption. However, adding a single node to large objects does not result in a significant increasing in their size. Therefore, changing the shape of the large objects has considerably more influence on the jamming density than increasing the object size. For example, jamming coverages for objects  $T_{11}$  and  $T_{27}$  from Table I are almost identical, although they are of different sizes. The presented results in Fig. 2 also suggest that there is no correlation between the order of symmetry axis  $n_s$  of the shape and the corresponding values of the jamming density  $\theta_j$ . It is interesting that, for the wrapping hexagons [Fig. 2(c)], the jamming density  $\theta_j$  reaches a local minimum for the most regular hexagons  $H_7$  and  $H_{19}$  with symmetry axis of sixth order,  $n_s = 6$ , while the jamming density  $\theta_j$  for object  $H_{16}$  of low symmetry order,  $n_s = 1$ , is greater than  $\theta_j$  for the wrapping hexagons that cover more than  $j = 11$  sites.

In order to gain a better insight into the complex kinetics of the adsorption processes of wrapping objects it is useful to analyze in particular the temporal evolution of probability for the insertion of a new particle onto a lattice. Insertion probability  $p_j$  for the object  $j$  at time  $t$  is calculated from the expression

$$p_j = 1 - \frac{c_j}{N}, \quad j = 1, 2, 3, \dots, 30, \quad (2)$$

where

$$c_j = \frac{1}{6} (6n_0^{(j)} + 5n_1^{(j)} + 4n_2^{(j)} + 3n_3^{(j)} + 2n_4^{(j)} + n_5^{(j)}). \quad (3)$$

Here  $n_k^{(j)}$  is the total number of sites at which the beginning of the walk that makes the shape  $j$  can be placed, whereby the deposited object  $j$  at each available site can be oriented in  $k$  ( $k = 0, \dots, 5$ ) different ways. We emphasize that the first step determines the orientation  $k$  of the object. In Eq. (2),  $N$  denotes the total number of lattice sites,  $N = L^2$ . The quantities  $n_k^{(j)}$ ,  $k = 0, 1, 2, 3, 4, 5$  are calculated numerically from the simulation data. Let us remark that a different choice of the head of the object (the beginning of the walk) does not change the value of the coefficient  $c_j$ . We have verified that usage of a different head for all examined objects gives quantitatively the same results for coefficients  $c_j$  and probabilities  $p_j$ .

Below we try to characterize quantitatively the time and density dependence of the insertion probability  $p_j$  during irreversible deposition of wrapping triangles  $T_j$ , rhombuses  $R_j$ , and hexagons  $H_j$ . In Fig. 3(a) the coefficients  $c_j$  [Eq. (3)] are plotted as a function of the number  $n$  of randomly deposited objects for all wrapping triangles  $T_j$  (Table I). Numerical simulations for wrapping rhombuses  $R_j$  and hexagons  $H_j$  (Tables II and III) produce qualitatively similar results for the evolution of coefficients  $c_j(n)$  during the deposition process. At very early times of the process, deposited objects do not “feel” the presence of the others, and  $c_j(n) = n c_j(1)$  for sufficiently low densities  $\theta$ . Therefore, at the very early times, the plot of the coefficients  $c_j$  with respect to  $n$  is linear on a double logarithmic scale with the slope 1. At higher densities, “excluded volumes” for deposited objects begin to overlap, leading to slowing of the linear growth of the coefficients  $c_j$  with  $n$ . In Fig. 3(b) we show the behavior of coefficients  $c_j(\theta)$  in the late stages of deposition process. As can be seen from Fig. 3(b), the final value  $N = L^2 = 57600$  of coefficients  $c_j$  is reached when the coverage  $\theta$  of the system approaches the jammed-state value  $\theta_j$ . The curves  $c_j(\theta)$  shift to lower

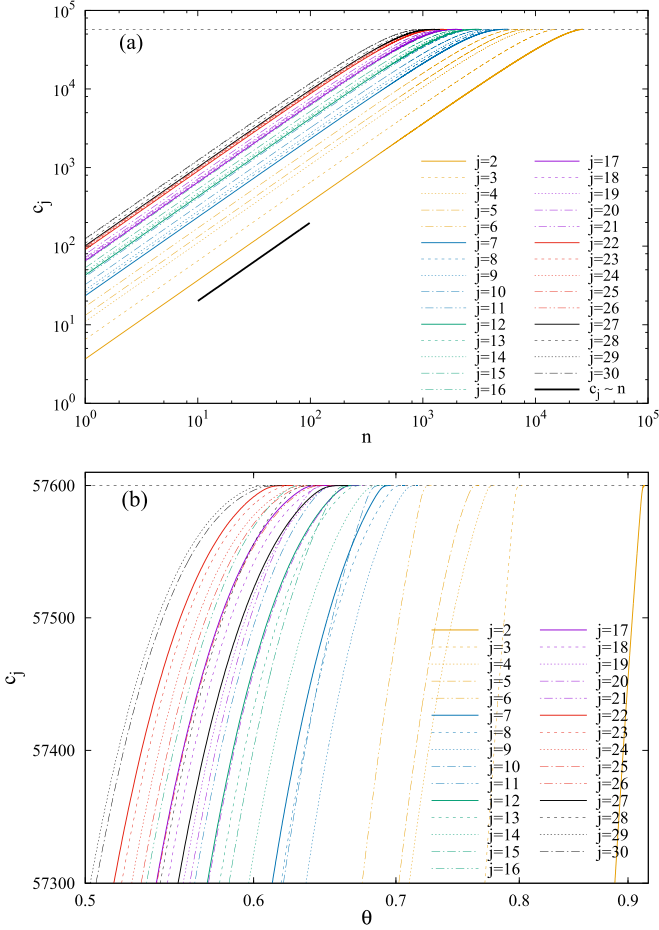


FIG. 3. The coefficients  $c_j$  [Eq. (3)] as a function (a) of the number  $n$  of deposited objects, and (b) of the coverage  $\theta$ , in the late stage of the deposition process, for all wrapping triangles  $T_j$  (Table I). The horizontal line represents the final value  $N = L^2 = 57600$  of the coefficients  $c_j$  that is reached when the coverage  $\theta$  approaches to the jamming limit  $\theta_j$ . The solid black line has slope 1 and is a guide for the eye.

densities  $\theta$  when the object size increases. Some of the lines  $c_j(\theta)$  intersect with the other ones in the late stage of the process when the influence of the shape on the densification kinetics becomes very important.

The results for the insertion probability  $p_j$  are shown in Fig. 4 for the same wrapping objects as in Fig. 1. Insertion probability  $p_j$  is a monotonically decreasing function of the coverage fraction  $\theta$  for all the shapes. When the coverage  $\theta$  approaches the jamming limit  $\theta_j$ , the probability  $p_j$  decreases very rapidly with  $\theta$  and vanishes at  $\theta_j$ .

### B. Properties of the insertion probability: Role of rotational symmetry of the shapes

In the following, we try to find a universal functional type that describes the decay of the insertion probability  $p_j$  for all shapes in a broad range of the coverage  $\theta$ . In addition, the proposed function  $p_j = f(\theta)$  should be consistent with the exponential approach of the coverage fraction  $\theta(t)$  to the jamming limit  $\theta_j$  [Eq. (1)]. Looking for a function that gives the best fit to probability  $p_j$ , we have tried a wide set of

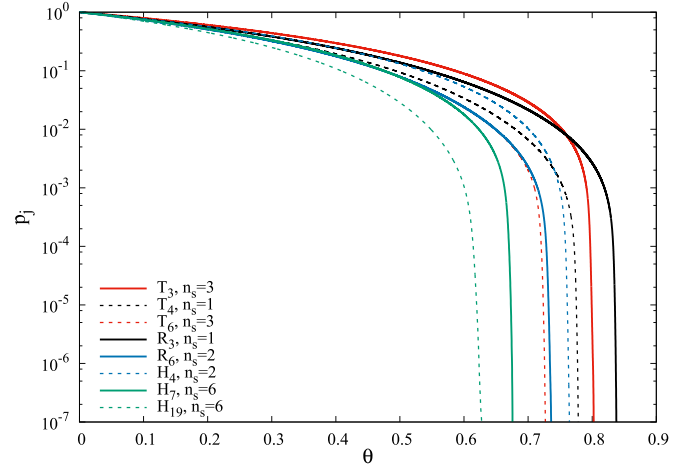


FIG. 4. Shown here is the insertion probability  $p_j$  vs the coverage  $\theta$  for triangles  $T_3$ ,  $T_4$ ,  $T_6$ , rhombuses  $R_3$ ,  $R_6$ , and hexagons  $H_4$ ,  $H_7$ ,  $H_{19}$  from Tables I–III.

phenomenological fitting functions for relaxation processes in many complex disordered systems [42]. The best agreement with our simulation data was obtained by the fitting function of the form

$$\begin{aligned} p_j(\theta) &= A \left(1 - \frac{\theta}{\theta_j}\right) \exp(-\lambda_1 \theta^{\lambda_2}) \\ &= A \left(1 - \frac{\theta}{\theta_j}\right) \exp \left[ - \left( \frac{\theta}{\theta^{(c)}} \right)^{\lambda_2} \right], \end{aligned} \quad (4)$$

where  $A$ ,  $\lambda_1$ , and  $\lambda_2$  are the fitting parameters, and

$$\theta^{(c)}(j) = [\lambda_1(j)]^{(-1/\lambda_2(j))}. \quad (5)$$

Parameter  $\theta^{(c)}(j)$  determines the characteristic density scale, and exponent  $\lambda_2$  measures the decay rate of the probability  $p_j(\theta)$  on this scale. Interestingly, Ludewig *et al.* [43] have proposed that the decrease of the grain mobility with the packing fraction during the granular compaction is well described by the empirical law of the form (4).

In Fig. 5 some representative results for the insertion probability  $p_j(\theta)$  are shown together with the fitting functions of the form (4). The fitting parameters are obtained by using the nonlinear fitting routine `FMINSEARCH` in `MATLAB`<sup>®</sup> (MathWorks, Natick, MA). This is an implementation of the Nelder-Mead simplex algorithm [44], which minimizes a nonlinear function of several variables. For each shape, a fitting procedure is carried out within a certain range of coverage  $\theta$  below  $\theta_j$ , where the probability  $p_j$  is lower than  $p_j^c = 0.15$ . The cutoff probability  $p_j^c = 0.15$  is chosen to provide a wide density range within which the fitting procedure is implemented for all wrapping shapes. For most shapes, the cutoff probability  $p_j^c = 0.15$  corresponds to the densities that are 30%–40% lower than the corresponding jamming limit  $\theta_j$ . We have verified that usage of different, but sufficiently small, values of the cutoff parameter  $p_j^c$  gives quantitatively similar results for fitting coefficients leading to qualitatively same conclusions.

The data for fitting parameters  $\lambda_1$  and  $\lambda_2$  for all wrapping triangles  $T_j$  from Table I are plotted in Fig. 6. The parameters

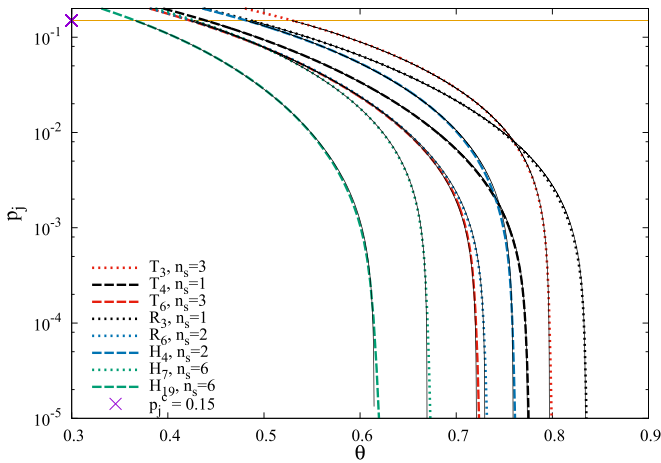


FIG. 5. The decay of the insertion probability  $p_j(\theta)$  for the same objects as in Fig. 4 in the range of coverage  $\theta$  where the corresponding probability  $p_j$  is lower than  $p_j^c = 0.15$  (thin horizontal line). The continuous superimposed lines are the fits according to Eq. (4). The fitting parameters  $\lambda_1$  and  $\lambda_2$  are reported in Fig. 6.

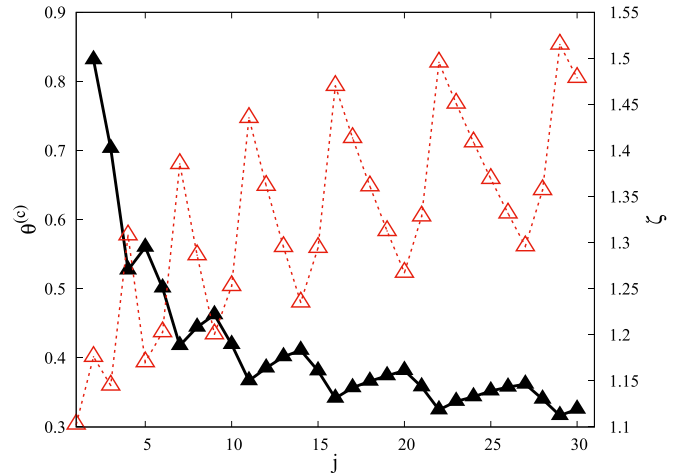


FIG. 7. Characteristic density  $\theta^{(c)}$  (Eq. (5)) for all wrapping triangles  $T_j$  from Table I (solid symbols, left-hand axis). The opened symbols are plotted against the right-hand axis and give the values of the shape factor  $\zeta(j)$  for all wrapping triangles  $T_j$ . The characteristic density  $\theta^{(c)}(j)$  is anticorrelated with the shape factor  $\zeta(j)$ .

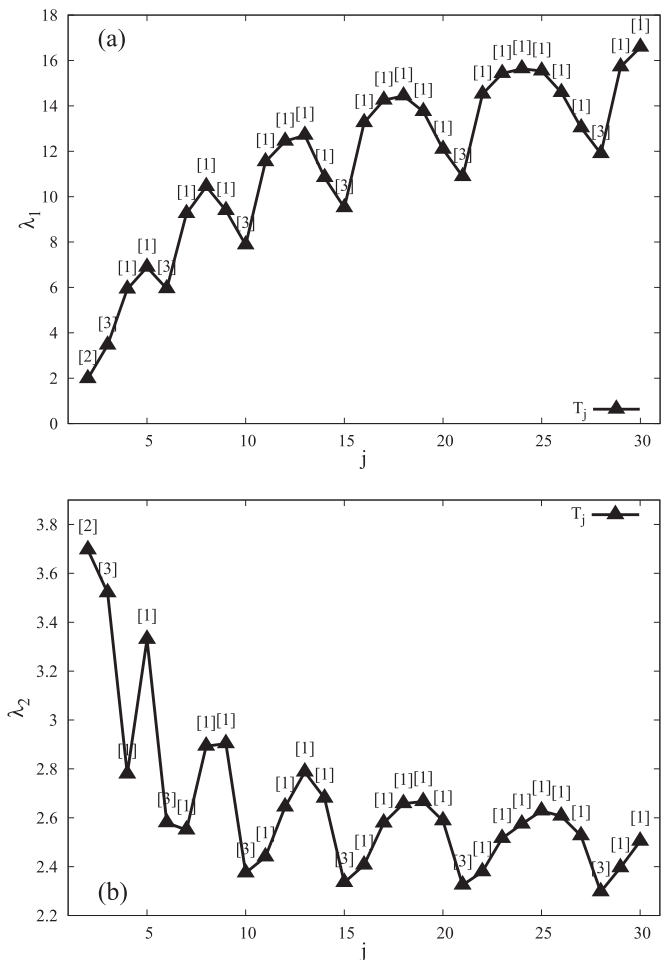


FIG. 6. Parameters (a)  $\lambda_1$  and (b)  $\lambda_2$  of the fit (4) for all wrapping triangles from Table I. Numerical values of the symmetry order  $n_s$  of the shape  $j$  are given in the square brackets above the corresponding plot symbols.

$\lambda_1$  and  $\lambda_2$  depend both on the symmetry order and on the size of the object. The size dependence of the fitting parameters is more pronounced for the parameter  $\lambda_1$ . However, the most striking feature is that the fitting parameters  $\lambda_1$  and  $\lambda_2$  exhibit a local minima for wrapping triangles of the highest symmetry order,  $n_s = 3$ . It is important to note that the fitting procedure for wrapping rhombuses  $R_j$  and hexagons  $H_j$  from Tables II and III produce qualitatively similar results for the dependence of the fitting parameters  $\lambda_1$  and  $\lambda_2$  both on the symmetry order  $n_s$  and on the size  $j$  of the object.

We have also considered the behavior of the characteristic density  $\theta^{(c)}$  [Eq. (5)] as a function of the object size  $j$ . Figure 7 shows the variation of the parameter  $\theta^{(c)}$  with  $j$  for all wrapping triangles  $T_j$ . It is obvious that the symmetry order  $n_s$  of the shape is not correlated with the characteristic density  $\theta^{(c)}(j)$  for various objects. The behavior of  $\theta^{(c)}(j)$  differs from case to case. For example, for shapes  $j = 4, 7, 11, 16, 22, 29$  formed by adding a node to the triangle of the highest symmetry order ( $n_s = 3$ ),  $\theta^{(c)}(j)$  has a local minima. On the other hand, for shapes  $j = 5, 9, 14, 20, 27$  formed by removing a node from the triangle of the highest symmetry order ( $n_s = 3$ ),  $\theta^{(c)}(j)$  has a local maxima.

Previous findings suggest that we should consider the connection of deposition kinetics with some of the new geometrical properties of the extended objects. For this purpose we use the concept of the shape factor, which is a dimensionless measure of deviation of the extended objects from circularity. Let us first mention the definition of the shape factor in the case of planar geometric figures. Shape factor  $\zeta$  (parameter of nonsphericity) combines the circumference  $C$  and the surface  $S$  of the planar figure [37,45]. It is defined as

$$\zeta = \frac{C^2}{4\pi S}. \quad (6)$$

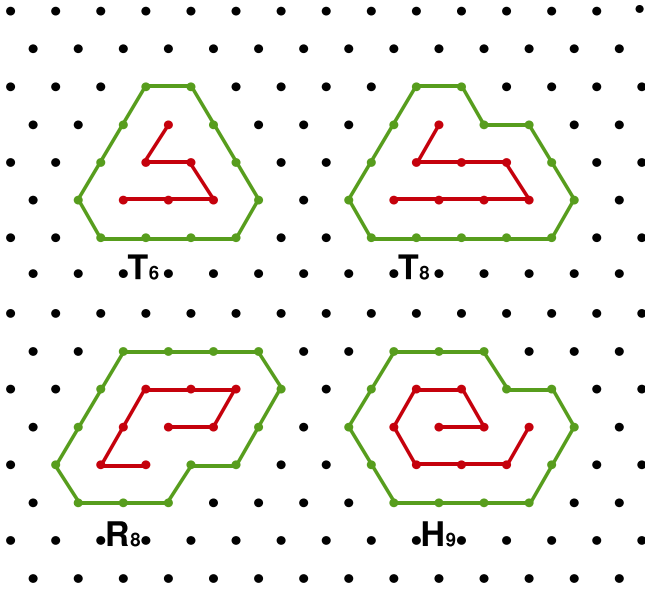


FIG. 8. Construction of the polygon determined by the first neighboring sites on the lattice for the wrapping triangles  $T_6$  and  $T_8$ , rhombus  $R_8$ , and hexagon  $H_9$ . The shape factor of the extended object is equal to the shape factor (6) of the polygon of the first neighboring sites on the lattice.

For a square  $\zeta = 4/\pi \approx 1.273$ , for a regular pentagon  $\zeta = \pi/5 \tan(\pi/5) \approx 1.156$ , and for a regular hexagon  $\zeta = 6/\sqrt{3\pi^2} \approx 1.103$ . Generally, for a regular  $N$ -sided polygon we have  $\zeta = (N/\pi) \tan(\pi/N)$ , which sets a lower bound for other  $N$ -sided polygons. Thus a circular structure has a shape factor  $\zeta = 1$ , while for a convex polygon, the more anisotropic is the polygon, the higher is  $\zeta > 1$ .

In the case of extended objects on a triangular lattice, the above definition of the shape factor (6) must be generalized. Each lattice shape can be surrounded by the first neighboring sites on the lattice. These nodes unambiguously define a polygon containing the given object. For example, the polygon of the first neighboring sites for a monomer ( $j = 1$ ) is a hexagon; the constructions of such polygon for wrapping triangles  $T_6$  and  $T_8$ , rhombus  $R_8$ , and hexagon  $H_9$  are shown in Fig. 8. Thus, the shape factor of the extended object is equal to the shape factor (6) of the polygon defined by the first neighboring sites on the lattice.

Values of the shape factor  $\zeta(j)$  for all wrapping triangles  $T_j$  are given in Fig. 7 together with the corresponding characteristic densities  $\theta^{(c)}(j)$ . We can see that  $\theta^{(c)}(j)$  increases with  $j > 2$  if  $\zeta(j)$  decreases and vice versa. In other words, positions of the local maxima (minima) of  $\theta^{(c)}(j)$  coincide with position of the local minima (maxima) of  $\zeta(j)$ . Qualitatively the same behavior of the shape factor  $\zeta(j)$  and the parameter  $\theta^{(c)}(j)$  is found in the cases of wrapping rhombuses  $R_j$  and hexagons  $H_j$ . Indeed, in Figs. 9 and 10 we show that the characteristic density  $\theta^{(c)}(j)$  is anticorrelated with the shape factor  $\zeta(j)$  for the wrapping rhombuses  $R_j$  and hexagons  $H_j$ .

Figure 11 illustrates that when the product between the shape factor and the characteristic density,  $\zeta(j) \times \theta^{(c)}(j)$ , is plotted as a function of the object size  $j$ , the data for wrapping triangles  $T_j$ , rhombuses  $R_j$ , and hexagons  $H_j$  collapse onto

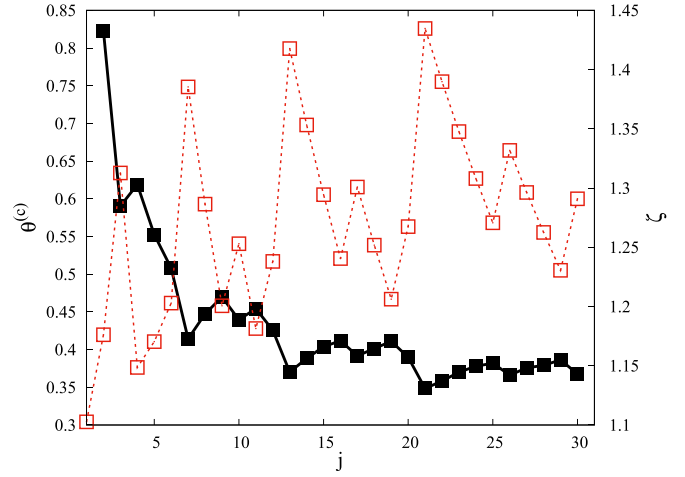


FIG. 9. Characteristic density  $\theta^{(c)}$  [Eq. (5)] for all wrapping rhombuses  $R_j$  from Table II (solid symbols, left-hand axis). The opened symbols are plotted against the right-hand axis and give the values of the shape factor  $\zeta(j)$  for all wrapping rhombuses  $R_j$ . The characteristic density  $\theta^{(c)}(j)$  is anticorrelated with the shape factor  $\zeta(j)$ .

a single curve. This figure demonstrates the existence of the single universal master function of the form

$$F(j) = \zeta(j) \times \theta^{(c)}(j) = 1 - C_1 \{1 - \exp[-\frac{1}{2}(j - 2)^{C_2}]\}, \quad (7)$$

where the two fitting parameters are  $C_1 = 0.525$  and  $C_2 = 0.685$ . This result strongly suggests that, for various objects of the same length, the characteristic density  $\theta^{(c)}(j)$  of more rounded shapes exceeds the  $\theta^{(c)}(j)$  of the elongated ones. Indeed, in Fig. 12 we show the parameter  $\theta^{(c)}$  as a function of the shape factor  $\zeta$  for various triplets of triangles, rhombuses, and hexagons ( $T_j, R_j, H_j$ ) of the same size,

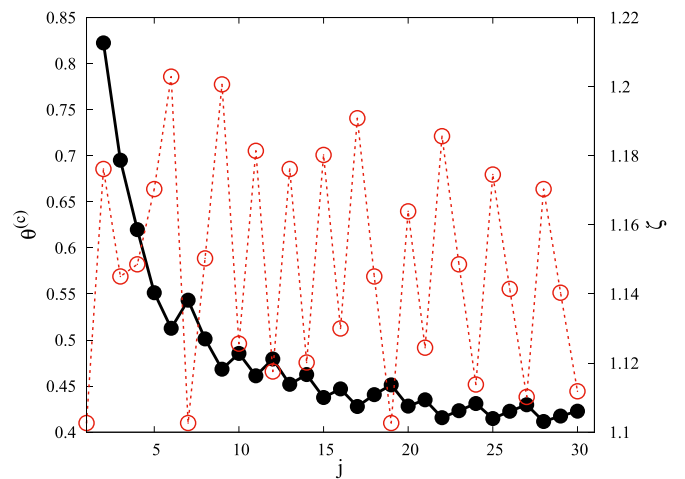


FIG. 10. Characteristic density  $\theta^{(c)}$  [Eq. (5)] for all wrapping hexagons  $H_j$  from Table III (solid symbols, left-hand axis). The opened symbols are plotted against the right-hand axis and give the values of the shape factor  $\zeta(j)$  for all wrapping hexagons  $H_j$ . The characteristic density  $\theta^{(c)}(j)$  is anticorrelated with the shape factor  $\zeta(j)$ .

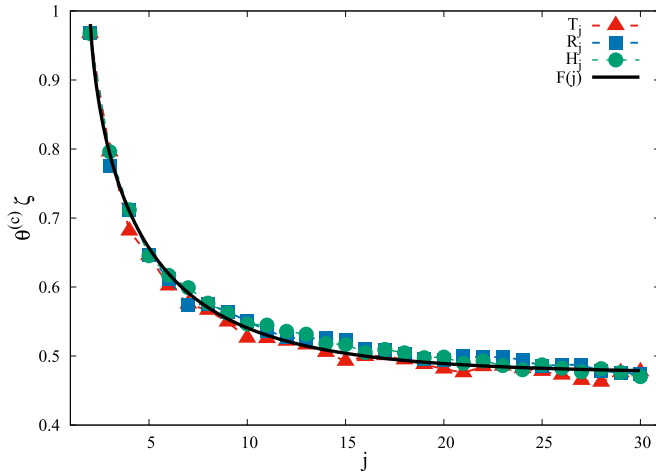


FIG. 11. The product between the shape factor and characteristic density,  $\zeta(j) \times \theta^{(c)}(j)$ , as a function of the object size  $j$  for all wrapping triangles  $T_j$ , rhombuses  $R_j$ , and hexagons  $H_j$  from Tables I–III. The black solid curve is the stretched exponential fit of Eq. (7).

$j = 14, 17, 19, 22, 25, 28, 30$ . For each triplet  $(T_j, R_j, H_j)$ , our data confirm that the parameter  $\theta^{(c)}$  decreases with the shape factor  $\zeta$ .

Now, it is necessary to establish a connection between the proposed fitting function  $p_j(\theta)$  [Eq. (4)] and the exponential approach of the coverage fraction  $\theta(t)$  to the jamming limit  $\theta_j$  [Eq. (1)]. It is easy to show that the following differential equation,

$$\frac{d\theta}{dt} = j p_j(\theta) = j A \left(1 - \frac{\theta}{\theta_j}\right) \exp \left[ - \left( \frac{\theta}{\theta^{(c)}} \right)^{\lambda_2} \right], \quad (8)$$

describes the temporal evolution of the coverage  $\theta(t)$  in the late stages of deposition process. Let  $\theta(t) = jn(t)/L^2$  be the fraction of total lattice sites covered by the deposited objects of

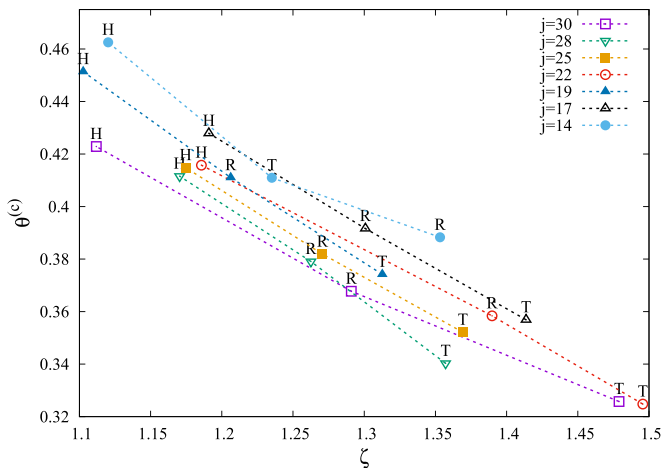


FIG. 12. Characteristic density  $\theta^{(c)}$  [Eq. (5)] as a function of the shape factor  $\zeta$  for various triplets of triangles, rhombuses and hexagons  $(T_j, R_j, H_j)$  of the same size,  $j = 14, 17, 19, 22, 25, 28, 30$ . The letter above the plot symbol indicates the object type. Sizes of the objects for the corresponding triplets are given in the legend.

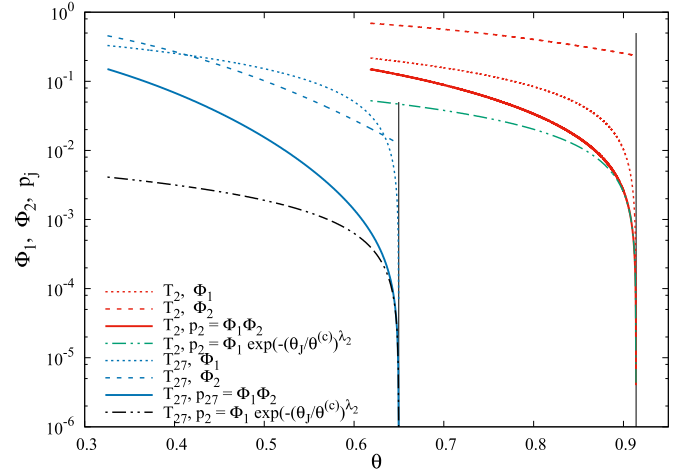


FIG. 13. Functions  $\Phi_1(\theta)$  and  $\Phi_2(\theta)$  [Eqs. (9) and (10)] obtained by fitting Eq. (4) to the insertion probability data for wrapping triangles  $T_2$  and  $T_{27}$  in the case of  $p_j^c = 0.15$ . The solid lines give the fitting function  $p_j(\theta) = \Phi_1(\theta)\Phi_2(\theta)$  [Eq. (4)]. The dot-dashed lines give the approximation  $p_j(\theta) = \Phi_1(\theta) \exp[-(\theta_j/\theta^{(c)})^{\lambda_2}]$ , as indicated in the legend. Approximation (11) is applicable in the narrower density range in the case of the large object  $T_{27}$  than in the case of the dimer  $T_2$ . The parameters of the fit (4) are  $\theta^{(c)} = 0.8313$ ,  $\lambda_2 = 3.6964$  for shape  $T_2$ , and  $\theta^{(c)} = 0.3619$ ,  $\lambda_2 = 2.5266$  for shape  $T_{27}$ . The thin vertical lines indicate the values of jamming coverage for shapes  $T_2$  ( $\theta_j = 0.9141$ ) and  $T_{27}$  ( $\theta_j = 0.6498$ ).

size  $j$  at time  $t$  [ $n(t)$  denotes the number of objects adsorbed at time  $t$ ]. Since the time  $t$  is counted by the number of adsorption attempts and scaled by the total number of lattice sites  $L^2$ , the number of deposited objects is increased by  $p_j L^2$  per unit time  $t \rightarrow t + 1$ . Therefore, the coverage at time  $t + 1$  is equal to  $\theta(t + 1) = j[n(t) + p_j L^2]/L^2$ , so that  $\theta(t + 1) - \theta(t) = j p_j$  is the increase of the coverage per unit time. Since  $\theta(t + 1) - \theta(t) \approx d\theta/dt$ , we get  $d\theta/dt = j p_j$ . Finally, we obtain Eq. (8) assuming that function (4) describes the decay of the insertion probability  $p_j$  for all shapes in a wide range of the coverage  $\theta$  just below  $\theta_j$ .

Unfortunately, differential equation (8) cannot be solved analytically. However, Eq. (8) can be simplified and solved if we restrict ourselves to the consideration of the very late-time behavior of the deposition process. The right side of differential Eq. (8) is proportional to the product between linear  $\Phi_1$  and stretched exponential function  $\Phi_2$ , which are given by

$$\Phi_1(\theta) = A \left(1 - \frac{\theta}{\theta_j}\right), \quad (9)$$

$$\Phi_2(\theta) = \exp \left[ - \left( \frac{\theta}{\theta^{(c)}} \right)^{\lambda_2} \right]. \quad (10)$$

There is a significant difference in the behavior of these functions near the jamming density for all examined objects. Figure 13 shows the functions  $\Phi_1(\theta)$  and  $\Phi_2(\theta)$  obtained by fitting Eq. (4) to the insertion probability data in the late stage of the deposition processes for wrapping triangles  $T_2$  and  $T_{27}$ . Since the time derivative of coverage  $d\theta/dt$  vanishes at  $t \rightarrow \infty$  and  $\Phi_2 \rightarrow \exp[-(\theta_j/\theta^{(c)})^{\lambda_2}] > 0$ ,  $t \rightarrow \infty$ , it is obvious that the function  $\Phi_1$  is essential for controlling the kinetics of

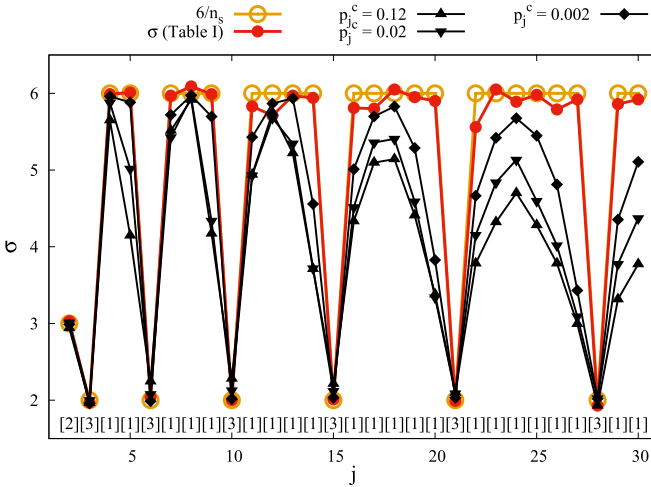


FIG. 14. Relaxation time  $\sigma$  calculated from the expression (13) for all wrapping triangles (Table I). Results are given for three values of threshold  $p_j^c = 0.12, 0.02, 0.002$ , as indicated in the legend. The full circles correspond to values of  $\sigma$  in Table I. Open circles correspond to values  $6/n_s(j)$  [Eq. (14)] for  $j = 2, \dots, 30$ . Numerical values of the symmetry order  $n_s(j)$  of the shape are given in the square brackets above the x axis.

adsorption process near the jamming limit  $\theta_j$ . Our further analysis deals with the rapidity of the approach to the jammed state, so that we can introduce the following approximation:

$$\Phi_2(\theta) = \exp\left[-\left(\frac{\theta}{\theta^{(c)}}\right)^{\lambda_2}\right] \approx \exp\left[-\left(\frac{\theta_j}{\theta^{(c)}}\right)^{\lambda_2}\right],$$

for  $\theta \lesssim \theta_j$ . (11)

This approximation allows us to solve Eq. (8). Accordingly, the coverage fraction of the system  $\theta$  grows exponentially in time towards the jamming state value  $\theta_j$ :

$$\theta(t) = \theta_j \left[1 - \exp\left(-\frac{t}{\sigma}\right)\right], \quad \text{for } \theta \lesssim \theta_j, \quad (12)$$

where

$$\sigma = \frac{\theta_j \exp(\lambda_1 \theta_j^{\lambda_2})}{jA} = \frac{\theta_j \exp\left[\left(\frac{\theta_j}{\theta^{(c)}}\right)^{\lambda_2}\right]}{jA}. \quad (13)$$

Consequently, the function (4) that we have proposed to characterize the insertion probability  $p_j$  is compatible with the exponential approach (1) to the jamming limit  $\theta_j$ .

Equation (13) is a functional relationship between the relaxation time  $\sigma$  and the parameters  $A, \lambda_1$ , and  $\lambda_2$  in the fitting function (4). Our previous findings concerning the kinetics of the deposition process clearly confirm that the relaxation time  $\sigma$  in Eq. (1) is inversely proportional to the order of symmetry axis  $n_s$  of the shape:

$$\sigma = \frac{6}{n_s}. \quad (14)$$

It is interesting to verify whether the Eq. (13) gives the values of the parameter  $\sigma$  that are in accordance with the symmetry order  $n_s$  of the shape [Eq. (14)]. Figure 14 shows the values of the relaxation time  $\sigma$  obtained from the expression (13) for all wrapping triangles (Table I). For each object, the values of the

parameters  $A, \lambda_1$ , and  $\lambda_2$  in Eq. (13) were calculated by fitting the function (4) to the insertion probability data for three values of the cutoff probability  $p_j^c = 0.12, 0.02, 0.002$ . It is obvious that Eqs. (13) and (14) give approximately equal relaxation times  $\sigma$  in the case of more symmetric shapes ( $n_s = 2, 3; j = 2, 3, 6, 10, 15, 21, 28$ ). However, the values of parameter  $\sigma$  obtained by Eq. (13) in the case of asymmetric shapes ( $n_s = 1$ ) are not well fitted by integer  $6/n_s = 6$  [Eq. (14)]. These deviations are particularly high for the large objects. The reasons for these differences can be seen in Fig. 13. Comparing the insertion probabilities near the jamming state for the objects  $T_2$  and  $T_{27}$ , one can see that approximation (11) is applicable in the narrower density range in the case of the large object  $T_{27}$  than in the case of the dimer  $T_2$ . Accordingly, the lowering of the cutoff value  $p_j^c$  reduces the deviation of the relaxation time  $\sigma$ , calculated from Eq. (13), from the integer value of 6 (see Fig. 14). The presented results provide a further justification for the choice of function (4) to describe the decay of the insertion probability  $p_j$  for all extended shapes on the triangular lattice.

#### IV. SUMMARY

RSA kinetics of particles of various shapes on flat two-dimensional homogeneous surfaces depends generally on the shape anisotropy and on the number of degrees of freedom. However, in the case of irreversible deposition on planar lattices, the kinetics of the late stage of deposition is determined exclusively with the symmetry properties of the shapes. To demonstrate this, we have performed extensive numerical simulations of the RSA using the shapes of different number of segments and rotational symmetries on a triangular lattice. The shapes are made by self-avoiding lattice steps, whereby the size of the objects is gradually increased by wrapping the walks in several different ways.

As expected, the approach to the jamming limit was found to be exponential for all the shapes. It was shown that the coverage kinetics is severely slowed with the decrease of the order of symmetry of the shape. We have also pointed out that the relaxation time  $\sigma$  [Eq. (1)] is inversely proportional to the order of symmetry axis  $n_s$  of the shape,  $\sigma = 6/n_s$ . We found that for small objects, jamming coverages  $\theta_j$  decrease very rapidly with the size of the objects, regardless of their shape. But for sufficiently large objects it turned out that changing the shape has considerably more influence on the jamming density than increasing the object size.

Special attention is paid to the behavior of probability  $p_j$  for the insertion of a new particle onto a lattice during the deposition process. The insertion probability  $p_j$  is found to decay with the coverage  $\theta$  according to Eq. (4). It is shown that the characteristic density  $\theta^{(c)}(j)$  [see Eq. (4)] is anticorrelated with the shape factor  $\zeta(j)$  of the objects. In addition, our data confirm that, for objects of the same length, parameter  $\theta^{(c)}$  decreases with the shape factor  $\zeta$ . Consequently, this work provides the link between the behavior of the insertion probability  $p_j$  and the intrinsic properties of the shapes.

We have established a connection between the proposed fitting function [Eq. (4)] for the decay of the insertion probability and the exponential approach of the coverage fraction  $\theta(t)$  to the jamming limit  $\theta_j$  [Eq. (1)]. It was shown

that the obtained functional relationship (13) between the relaxation time  $\sigma$  and the fitting parameters in expression (4) gives the values of the parameter  $\sigma$  that are in accordance with the symmetry order  $n_s$  of the shape [Eq. (14)].

It must be stressed that the presence of desorption and diffusional relaxation of particles changes some of the important properties of the RSA. When desorption is introduced in RSA processes, slowing of the deposition dynamics occurs with increasing of symmetry order of the shapes [29]. Furthermore, the presence of diffusion only hastens the approach to the final disordered state [32]. As expected, the behavior of the insertion probability during the reversible deposition of extended objects look very different in comparison with the irreversible case. When desorption of the objects is present, insertion probability first follows the corresponding RSA

curve until it reaches a value close to the equilibrium one at which point it plateaus and evolves very weakly towards the equilibrium [46]. Consequently, function (4) is not suitable to describe the decreasing of the insertion probability toward its equilibrium value during the reversible RSA.

## ACKNOWLEDGMENTS

This work was supported by the Ministry of Education, Science, and Technological Development of the Republic of Serbia under Projects ON171017 and III45016, and by the European Commission under H2020 project VI-SEEM, Grant No. 675121. Numerical simulations were run on the PARADOX supercomputing facility at the Scientific Computing Laboratory of the Institute of Physics Belgrade.

- 
- [1] J. W. Evans, Random and cooperative sequential adsorption, *Rev. Mod. Phys.* **65**, 1281 (1993).
- [2] V. Privman (ed.), *Nonequilibrium Statistical Mechanics in One Dimension* (Cambridge University Press, Cambridge, UK, 1997), (a collection of review articles).
- [3] V. Privman, guest editor, *Colloids Surf. A* **165**, 1 (2000), (a collection of review articles).
- [4] A. Cadilhe, N. A. M. Araújo, and V. Privman, Random sequential adsorption: From continuum to lattice and pre-patterned substrates, *J. Phys.: Condens. Matter* **19**, 065124 (2007).
- [5] J. Feder, Random sequential adsorption, *J. Theoret. Biol.* **87**, 237 (1980).
- [6] R. H. Swendsen, Dynamics of random sequential adsorption, *Phys. Rev. A* **24**, 504 (1981).
- [7] Y. Pomeau, Some asymptotic estimates in the random parking problem, *J. Phys. A: Math. Gen.* **13**, L193 (1980).
- [8] B. Bonnier, Random sequential adsorption of binary mixtures on a line, *Phys. Rev. E* **64**, 066111 (2001).
- [9] M. C. Bartelt and V. Privman, Kinetics of irreversible multilayer adsorption: One-dimensional models, *J. Chem. Phys.* **93**, 6820 (1990).
- [10] S. S. Manna and N. M. Švrakić, Random sequential adsorption: Line segments on the square lattice, *J. Phys. A: Math. Gen.* **24**, L671 (1991).
- [11] Lj. Budinski-Petković and U. Kozmidis-Luburić, Random sequential adsorption on a triangular lattice, *Phys. Rev. E* **56**, 6904 (1997).
- [12] Lj. Budinski-Petković, S. B. Vrhovac, and I. Lončarević, Random sequential adsorption of polydisperse mixtures on discrete substrates, *Phys. Rev. E* **78**, 061603 (2008).
- [13] P. Viot, G. Tarjus, S. M. Ricci, and J. Talbot, Random sequential adsorption of anisotropic particles. I. Jamming limit and asymptotic behavior, *J. Chem. Phys.* **97**, 5212 (1992).
- [14] J. D. Sherwood, Random sequential adsorption of lines and ellipses, *J. Phys. A* **23**, 2827 (1990).
- [15] R. D. Vigil and R. M. Ziff, Random sequential adsorption of unoriented rectangles onto a plane, *J. Chem. Phys.* **91**, 2599 (1989).
- [16] R. D. Vigil and R. M. Ziff, Kinetics of random sequential adsorption of rectangles and line segments, *J. Chem. Phys.* **93**, 8270 (1990).
- [17] M. Cieřla and J. Barbasz, Random packing of regular polygons and star polygons on a flat two-dimensional surface, *Phys. Rev. E* **90**, 022402 (2014).
- [18] M. Cieřla and P. Karbowiczek, Random sequential adsorption of starlike particles, *Phys. Rev. E* **91**, 042404 (2015).
- [19] M. Cieřla, Continuum random sequential adsorption of polymer on a flat and homogeneous surface, *Phys. Rev. E* **87**, 052401 (2013).
- [20] P. B. Shelke and A. V. Limaye, Dynamics of random sequential adsorption (RSA) of linear chains consisting of  $n$  circular discs: role of aspect ratio and departure from convexity, *Surf. Sci.* **637–638**, 1 (2015).
- [21] M. Cieřla, Properties of random sequential adsorption of generalized dimers, *Phys. Rev. E* **89**, 042404 (2014).
- [22] M. Cieřla, G. Pajk, and R. M. Ziff, Shapes for maximal coverage for two-dimensional random sequential adsorption, *Phys. Chem. Chem. Phys.* **17**, 24376 (2015).
- [23] M. Cieřla, G. Pajk, and R. M. Ziff, In a search for a shape maximizing packing fraction for two-dimensional random sequential adsorption, *J. Chem. Phys.* **145**, 044708 (2016).
- [24] M. D. Khandkar, A. V. Limaye, and S. B. Ogale, Shape Effects in Random Sequential Adsorption of Zero-Area Angled Objects on a Continuum Substrate, *Phys. Rev. Lett.* **84**, 570 (2000).
- [25] G. C. Barker and M. J. Grimson, Random sequential adsorption of lattice shapes onto a square lattice, *Mol. Phys.* **63**, 145 (1988).
- [26] Lj. Budinski-Petković and U. Kozmidis-Luburić, Jamming configurations for irreversible deposition on a square lattice, *Physica A* **236**, 211 (1997).
- [27] R. S. Ghaskadvi and M. Dennin, Reversible random sequential adsorption of dimers on a triangular lattice, *Phys. Rev. E* **61**, 1232 (2000).
- [28] Lj. Budinski-Petković and U. Kozmidis-Luburić, Adsorption-desorption processes of extended objects on a square lattice, *Physica A* **301**, 174 (2001).
- [29] Lj. Budinski-Petković, M. Petković, Z. M. Jakšić, and S. B. Vrhovac, Symmetry effects in reversible random sequential adsorption on triangular lattice, *Phys. Rev. E* **72**, 046118 (2005).
- [30] V. Privman, Dynamics of nonequilibrium deposition, *Colloids Surf. A* **165**, 231 (2000).

- [31] C. Fusco, P. Gallo, A. Petri, and M. Rovere, Random sequential adsorption and diffusion of dimers and  $k$ -mers on a square lattice, *J. Chem. Phys.* **114**, 7563 (2001).
- [32] I. Lončarević, Z. M. Jakšić, S. B. Vrhovac, and Lj. Budinski-Petković, Irreversible deposition of extended objects with diffusional relaxation on discrete substrates, *Eur. Phys. J. B* **73**, 439 (2010).
- [33] G. Kondrat, Impact of composition of extended objects on percolation on a lattice, *Phys. Rev. E* **78**, 011101 (2008).
- [34] Lj. Budinski-Petković, I. Lončarević, M. Petković, Z. M. Jakšić, and S. B. Vrhovac, Percolation in random sequential adsorption of extended objects on a triangular lattice, *Phys. Rev. E* **85**, 061117 (2012).
- [35] N. I. Lebovka, Y. Yu. Tarasevich, D. O. Dubinin, V. V. Laptev, and N. V. Vygornitskii, Jamming and percolation in generalized models of random sequential adsorption of linear  $k$ -mers on a square lattice, *Phys. Rev. E* **92**, 062116 (2015).
- [36] J.-S. Wang and R. B. Pandey, Kinetics and Jamming Coverage in a Random Sequential Adsorption of Polymer Chains, *Phys. Rev. Lett.* **77**, 1773 (1996).
- [37] F. Moučka and I. Nezbeda, Detection and Characterization of Structural Changes in the Hard-Disk Fluid Under Freezing and Melting Conditions, *Phys. Rev. Lett.* **94**, 040601 (2005).
- [38] E. L. Hinrichsen, J. Feder, and T. Jssang, Geometry of random sequential adsorption, *J. Stat. Phys.* **44**, 793 (1986).
- [39] J. W. Evans, D. R. Burgess, and D. K. Hoffman, Irreversible random and cooperative processes on lattices: Spatial correlations, *J. Math. Phys.* **25**, 3051 (1984).
- [40] B. Bonnier, M. Hontebeyrie, Y. Leroyer, C. Meyers, and E. Pommiers, Adsorption of line segments on a square lattice, *Phys. Rev. E* **49**, 305 (1994).
- [41] N. I. Lebovka, N. N. Karmazina, Y. Yu. Tarasevich, and V. V. Laptev, Random sequential adsorption of partially oriented linear  $k$ -mers on a square lattice, *Phys. Rev. E* **84**, 061603 (2011).
- [42] R. Hilfer, Analytical representations for relaxation functions of glasses, *J. Non-Cryst. Solids* **305**, 122 (2002).
- [43] F. Ludewig, N. Vandewalle, and S. Dorbolo, Compaction of granular mixtures, *Granular Matter* **8**, 87 (2006).
- [44] J. C. Lagarias, J. A. Reeds, M. H. Wright, and P. E. Wright, Convergence properties of the Nelder-Mead simplex method in low dimensions, *SIAM J. Opt.* **9**, 112 (1998).
- [45] P. Richard, J. P. Troadee, L. Oger, and A. Gervois, Effect of the anisotropy of the cells on the topological properties of two- and three-dimensional froths, *Phys. Rev. E* **63**, 062401 (2001).
- [46] J. Talbot, G. Tarjus, and P. Viot, Adsorption-desorption model and its application to vibrated granular materials, *Phys. Rev. E* **61**, 5429 (2000).